

# IMPLEMENTATION AND VALIDATION OF A SURFACE TENSION MODEL FOR THE MULTI-SCALE APPROACH GENTOP

**G. Montoya**<sup>1,2</sup>, **E. Baglietto**<sup>1</sup>

<sup>1</sup> Nuclear Science and Engineering Department, Massachusetts Institute of Technology, 77  
Massachusetts Avenue, Cambridge MA 02139-4307, USA  
gmontoya@mit.edu; emiliob@mit.edu

**D. Lucas**<sup>2</sup>

<sup>2</sup> Helmholtz-Zentrum Dresden - Rossendorf, Institute of Fluid Dynamics, Bautzner Landstrasse  
400, 01328 Dresden, Germany  
d.lucas@hzdr.de

## ABSTRACT

Multiphase flows encountered in the nuclear industry are largely of a complex nature, and knowledge of the accurate distribution of the void fraction is of utmost importance for operation of the reactor under steady, transient, and accident conditions. At high void fractions, strong coalescence leads to the formation of large deformable bubbles. An appropriate multiphase CFD modeling of these flow regimes should be able to account for both, large and small interfacial structures, also including the effect on closure modeling of the large structures. A concept known as GEneralized TwO Phase flow or GENTOP, has been developed at the Helmholtz-Zentrum Dresden-Rossendorf in order to address such flow configurations, by dealing with a resolved potentially-continuous gas field, one or more polydispersed gas fields, and a continuous liquid phase. Application of the model to churn-turbulent and slug flow in vertical pipes [1], have evidenced an important limitation related to the lack of a surface tension modeling within the free surface, which leads to an unphysical accumulation of void near the pipe wall. This work discusses the implementation of surface tension and contact angle within the GENTOP approach, as well as the validation of these models against analytical and experimental results. The validation of the surface tension has been performed against analytically calculated oscillating periods of different shapes of ethanol droplets suspended in air. Furthermore, different contact angles are analyzed for a drop of water residing on a smooth surface. Rising velocities and deformation of a single large bubble rising in a vertical pipe were finally validated against analytical solutions. The implementation of the surface tension model in the GENTOP approach demonstrated improvements on the resolution of the bubble and stability of the interface, with considerable reduction of the numerical diffusion.

## KEYWORDS

CFD, GENTOP, Surface Tension, Contact Angle, MT-Loop

## 1. INTRODUCTION

In the nuclear industry, the ability of accurately modeling different flow regimes, ranging from low to high void fraction conditions is of utmost importance. For example, in Boiling Water Reactors (BWR) the knowledge of the correct distribution of the void fraction in the fuel assembly has a direct impact in the prediction of moderator density curves for neutronics calculations as well as on the heat transfer within the reactor fuel.

Most of the experimental and theoretical work has been largely focused on low gas volume fractions. The CFD modeling of bubbly flows, where the interfacial scales are expected to be smaller than the grid size, has more or less successfully relied on the Euler-Euler two-fluid approach. Due to the averaging procedure of the conservation equations, all information on the interfacial interaction is lost, and must be reintroduced in the form of closure relations. The available closure correlations for bubbly flow regimes have been tested on a wide range of cases and have shown reasonable agreement with experimental data [2].

The complexity of the two-phase flow increases with the void fraction. Here coalescence of small bubbles into larger ones leads to a higher level of complexity for the interface behavior which strongly interacts with the turbulent liquid phase. The resulting deformability makes the theoretical modeling of large bubbles especially difficult. When trying to address high void fraction flow regimes in which the interfacial scales are significantly larger than the grid size, while for annular flows interface tracking methods have been effectively tested, no general solution exists for churn-turbulent and slug flows where a mixture of small and large interfacial scales occurs. A hybrid approach, known as GENeralized TwO Phase flow or GENTOP [3] has been developed at the Helmholtz-Zentrum Dresden-Rossendorf, with the specific aim to challenge complex multiphase flows with a large variations of interfacial characteristics.

The GENTOP concept represents an extension to the Inhomogeneous MULTiple Size Group (iMUSIG) model [2], which allows tracking explicitly the existence and interaction of different bubble size groups, each with its own velocity field. The concept of GENTOP is based on the introduction of the explicit resolution of those gas structures that are considerably larger than the computational mesh adopted. Leveraging the polydispersed gas approach, bubble breakup and coalescence allows transfer between different size structures, while the modeling of mass transfer between the dispersed and continuous gas, allows transitioning between different morphologies depending of the flow situation. The GENTOP model has been qualitatively validated against a series of well-known cases, such as dam-break, impinging jets, and bubble columns. More recently, the model has also been quantitatively tested against vertical co-current adiabatic pipe flow cases under churn-turbulent and slug flow regimes [1]. The results of the validation exercises have evidenced shortcomings related to the absence of surface tension in the model, which lead to unphysical accumulation of void fraction at the wall-cells. The objective of this paper is to present the implementation of the surface tension and wall adhesion models in the GENTOP framework to improve the resolution of large structures in high void fraction flow regimes.

## 2. COMPUTATIONAL FLUID DYNAMICS (CFD) MODEL FORMULATION

The conservation equations solved in the Euler-Euler modeling approach are shown in Eq. 1 and Eq. 2, for mass and momentum respectively.

$$\frac{\partial(\alpha_k \rho_k)}{\partial t} + \nabla \cdot (\rho_k \alpha_k \mathbf{U}_k) = m_k''' \quad (1)$$

$$\begin{aligned} \frac{\partial(\alpha_k \rho_k \mathbf{U}_k)}{\partial t} + \nabla \cdot (\rho_k \alpha_k \mathbf{U}_k \mathbf{U}_k) \\ = -\alpha_k \nabla p_k + \nabla \cdot (\alpha_k \underline{\underline{\tau}}_k) + \rho_k \alpha_k \mathbf{g} + \sum_j \mathbf{M}_{kj}^i + \sum_m m_{m,k}''' \mathbf{U}_m \end{aligned} \quad (2)$$

Where  $m_k''' = \sum_m m_{m,k}'''$ , and  $\alpha_k$  represents the volume fraction of the field-k, while  $m_{m,k}'''$  is the volumetric mass transfer term from other fields which represents the same phase into field-k. The term  $\underline{\underline{\tau}}_k = \underline{\underline{\tau}}_k^\mu + \underline{\underline{\tau}}_k^{Re} = \mu_k (\nabla \mathbf{U}_k + \nabla \mathbf{U}_k^T) - \frac{2}{3} \mu_k \nabla \cdot \mathbf{U}_k \mathbf{I}$  is the total shear stress term. The variable  $\mathbf{M}_{kj}^i$  represents the interfacial momentum transfer per unit time between two different fields.

## 2.1. Polydispersed Modeling: Description of the Mechanistic Models for Interfacial Forces

The interfacial forces acting at the interface of the polydispersed field, are divided into drag and non-drag components. The interfacial non-drag forces taken into account in the simulations presented here are lift, wall, and turbulent dispersion forces.

The drag contribution model used in this paper is given in Eq. 3, and the drag coefficient is calculated as proposed by Ishii and Zuber with its proper swarm factor correction [4].

$$\mathbf{M}_{d,k}^D = \frac{3}{4} \alpha_{d,k} \frac{\rho_c}{d_b} C_{D,k} |\mathbf{v}_c - \mathbf{v}_{d,k}| (\mathbf{v}_c - \mathbf{v}_{d,k}) \quad (3)$$

The interfacial lift force between the continuous and dispersed phases is calculated as in Eq. 4. The lift coefficient ( $C_{L,k}$ ) is calculated as proposed by Tomiyama [5].

$$\mathbf{M}_{d,k}^L = -C_{L,k} \rho_c \alpha_{d,k} (\mathbf{v}_{d,k} - \mathbf{v}_c) \times (\nabla \times \mathbf{v}_c) \quad (4)$$

The interfacial wall force has been calculated as proposed by Tomiyama [6]. The wall coefficient ( $C_w$ ) has been implemented as proposed by Hosokawa [7] and is valid for high and low Morton numbers provided that the bubble does not collide with the wall. The turbulent dispersion is derived from the Favre Averaged Drag model [8]. Finally, the turbulent effect induced by the bubbles on the continuous liquid phase has been taken into account by implementing two additional source terms describing the bubble effects for  $k$  and  $w$ -equations proposed by Rzehak and Krepper [2].

## 2.2. The GENTOP -concept

The GEneralized TwO Phase flow or GENTOP concept has been recently developed, and validated against a large number of cases. Presently the GENTOP implementation consists of a continuous liquid phase  $l$ , a polydispersed gas phase  $dg$ , and a continuous gas phase  $cg$ . While the basis of the concept and latest improvements are discussed in this section, further detail information about it can be found in [1] and [3].

### 2.2.1 The inhomogeneous MUSIG approach

The bubble population balance approach known as Inhomogeneous Multiple Size Group (iMUSIG) proposed by Krepper [2], has been used for the small-scale dispersed gas phase. The MUSIG concept allows a division of the dispersed phase into a number of  $N$  velocity groups, where each velocity group is characterized by its own velocity field. Furthermore, this population balance model considers bubble coalescence and breakup into the sub-size groups, which means that the mass exchange between these sub-size groups can also exceed the size ranges assigned to the velocity clusters.

The GENTOP –concept has been developed in principle as an extension of this approach by adding a continuous gas phase. The mass transfer between dispersed and continuous gas is modelled depending on the flow situation, and the last velocity group included within the iMUSIG framework is considered as the new continuous gas. This velocity group represents all gas structures which are larger to an equivalent spherical bubble limit diameter  $d_{dg,max}$ .

### 2.2.2 Tracking of the interface

In order to be able to resolve the gas structures within the GENTOP concept, the first step is to localize the interface. An appropriate blending function  $\varphi_{fs}$  is used in order to identify the local interfacial structure.

Due to the averaged treatment of the Euler-Euler approach, the expected volume fraction discontinuity at the interface has been replaced by a gradient of volume fraction. For that reason, a free surface region is defined using the volume fraction gradient of the continuous gas  $|\nabla\alpha_{cg}|$ . The interface between the gas and the liquid is characterized by a variation of the volume fraction of  $\nabla\alpha_{cg}$  from 0 to 1 over a number of  $n$  grid cells of a  $\Delta x$  size, which leads to a critical value  $|\nabla\alpha_{cg}|_{crit} = 1/(n\Delta x)$  that allows a definition of the interface. The free surface function is defined as in Eq. 5.

$$\varphi_{fs} = 0.5 \tanh \left[ a_{fs} \Delta x \left( |\nabla\alpha_{cg}| - |\nabla\alpha_{cg}|_{crit} \right) \right] + 0.5 \quad (5)$$

### 2.2.3 Clustering-method

A clustering force has to be defined, in order to consider transitions from the dispersed towards the continuous gas phase using an aggregative effect within the volume fraction of the continuous gas. The clustering influence has been defined as an additional interfacial force acting exclusively between the continuous gas and liquid phases and it is included within the interfacial momentum transfer. This force acts proportionally to the gradient of the volume fraction of the liquid, as given in Eq. 6.

$$\mathbf{M}_l^{clust} = -\mathbf{M}_{cg}^{clust} = c_{clust} \varphi_{clust} \rho_l \nabla \alpha_l \quad (6)$$

While the original formulation [3] of GENTOP used a critical value of volume fraction to activate the clustering method, this was later found to be inconsistent, resulting for example in clustering effect within the free surface region and leading to destabilization of the interface. The current implementation is applied consistently with the critical gradient of volume fraction of the gas and with the  $\varphi_{fs}$  formulation. As shown in Eq. 7, the force acts outside the interface region, agglomerating the gas, and blends out as soon as the critical gradient of volume fraction appears, completely disappearing as soon as a fully formed interface occurs ( $\varphi_{fs} = 1$ ). The formulation also enforces the clustering to disappear within the continuous structure.

$$\varphi_{clust} \begin{cases} 1 & \text{if } \varphi_{fs} < 0.5 \\ 0.5 * \left( \tanh \left( 10 * (0.6 - \varphi_{fs}) \right) + 0.5 \right) & \text{if } 1 < \varphi_{fs} \leq 0.5 \\ 0 & \text{if } \varphi_{fs} = 1 \text{ or } \alpha_{cg} > 0.5 \end{cases} \quad (7)$$

The constant defined as  $c_{clust}$  was originally proposed to be adaptable to flow regime variations. The validation work has instead indicated that the full clustering force is suitable for very different flow conditions. A constant value of  $c_{clust} = 1$  is therefore recommended for the GENTOP application.

### 2.2.3 Interfacial transfer

In order to define an accurate interfacial transfer model depending on the corresponding amount of volume fraction presented, transitions between dispersed and continuous gas must be considered. This can be achieved by detecting the local gaseous morphology and by using a similar concept to that of the AIAD-model [9]. A transition approach between the closure models is defined by introducing new formulations for the interfacial area density  $A_D$  and drag coefficient  $C_D$  in order to consider free surfaces for the interfacial transfer of mass and momentum.

While the original formulation for the morphology transition adopted critical value of void fraction equal to 0.3, which represent the upper limit for bubbly flow conditions, this was later eliminated, as a more general formulation can be adopted for the morphology switch criterion,  $\varphi_{morph}$ , as given in Eq. 8.

$$\varphi_{morph} \begin{cases} 0 & \text{if } \varphi_{fs} < 0.5 \\ 0.5 * \left( \tanh \left( -5 * (0.5 - \varphi_{fs}) \right) + 0.5 \right) & \text{if } 0.5 \leq \varphi_{fs} < 1.0 \text{ or } \alpha_{cg} \geq 0.5 \\ 1 & \text{if } \varphi_{fs} = 1.0 \text{ or } \alpha_{cg} > 0.5 \end{cases} \quad (8)$$

Based on the blending function  $\varphi_{morph}$ , the formulations for interfacial area density and drag are defined in Eq. 9 and Eq. 10.

$$C_{D,cg} = (1 - \varphi_{morph})C_{D,bubb} + \varphi_{morph}C_{D,cont} \quad (9)$$

$$A_{D,cg} = (1 - \varphi_{morph})A_{D,bubb} + \varphi_{morph}A_{D,cont} \quad (10)$$

### 2.2.3 Coalescence for the continuous and dispersed gas phases

A special coalescence method for complete gaseous mass transfer is included in the model and represents a practical approach to enforce complete coalescence inside a resolved gas structure. This is a simple approach, to enforce the basic principle that small bubbles cannot occupy the same space where large gas structures exist. For the dispersed gas, represented by bubble sizes lower than  $d_{ggmax}$ , the coalescence mechanism is modeled as proposed by Prince and Blanch [10] taking into account the collision frequency of the bubbles and the efficiency of collision based on the film drainage model. Breakup mechanism are related to the impact of turbulent eddies on bubble surfaces using the model developed by Luo and Svendsen [11] which is based on the theory of isotropic turbulence. In that model, the occurrence of breakage is determined by the energy of oncoming eddies, which can participate in the bubble's deformation and breakup, only if their size is smaller than the bubble diameter. Intensity rates are added to the mass transfer rates in these models to harmonize the calculated results with experimental data. These are set as dimensionless factors  $F_C$  for coalescence and  $F_B$  for breakup. In the present calculations only the breakup coefficient has been lowered to 0.5, due to the high overprediction of breakup rates [2].

### 2.3. Surface Tension and Wall Adhesion Implementation for the GENTOP -concept

When fluid molecules are on or near a liquid surface, they experience uneven molecular attraction forces, which causes the liquid surfaces to possess an elastic strength. This is known as surface tension, and since abrupt changes occurs in the molecular forces when the fluid properties change discontinuously, it is considered an inherent characteristic of the material interfaces. This force exerts itself on fluid elements at interfaces in both the normal and tangential directions.

Brackbill [12], proposed the Continuum Surface Force (CSF) method for modeling surface tension in CFD. This approach implements the surface tension as a three-dimensional volumetric effect across an interface, rather than a boundary condition on the interface. While other methods exist such as the Continuum Surface Stress (CSS), the Ghost Fluid Method (GFM) and the Continuum Surface Tension (CST), for this study we have chosen to implement the CSF methods, especially due to the difficulties that other methods suffer when modeling topologically complex interfaces. For a curved interface, the surface tension as proposed by Brackbill [12] can be separated into a normal and tangential component as shown in Eq. 11.

$$M^{ST} = M^{ST}_n + M^{ST}_t \quad (11)$$

Where the normal component is given by Eq. 12.

$$\mathbf{M}^{ST}_n = \sigma * \kappa_n \quad (12)$$

Here,  $\sigma$  represents the surface tension coefficient, and  $n$  is the unit vector to the free surface directed from the main to the secondary fluid. The mean curvature of the free surface is given by  $k$ .

The tangential component, also known as the Marangoni effect, acts exclusively when the force varies along the surface, which is generally caused by temperature gradients. For a constant surface tension coefficient, the tangential force is zero, and the surface tension force works only normal to the interface.

In the CSF model, a smooth field of the primary phase volume fraction is used to calculate a vector normal to the interface ( $n = \nabla\alpha_i$ ). The curvature of the interface is then calculated in terms of the divergence of the normal vector. The normal component of the surface tension force is given by Eq. 13.

$$\mathbf{M}^{ST}_n = -\sigma * \nabla \cdot \left( \frac{\nabla\alpha_i}{|\nabla\alpha_i|} \right) * \nabla\alpha_i \quad (13)$$

Wall adhesion, on the other hand, describes the forces acting on the fluid interface along the line of contact with a solid wall. Complex microscopic phenomena acts in this region, resulting in an angle of equilibrium  $\theta_w$ . This angle is function of different surface free energies, which are characteristic of the different interfaces such as  $\gamma_{SL}$  for the solid-liquid interface,  $\gamma_{LG}$  for the liquid-gas interface, and  $\gamma_{SG}$  for the solid-gas interface. The contact angle,  $\theta_w$ , characterizes the wetting of the wall by the fluid where wetting occurs for  $\theta_w < 90^\circ$ , and non-wetting for  $\theta_w > 90^\circ$ . For that matter, the contact angle is not an intrinsic property of the fluid, but depends of the contact system. In order to account for the wall adhesion, a modification to the average normal vector at nodes in contact with the wall is made. The normal vector,  $n$ , which is used in order to compute the surface tension forces, needs to be modified at each node belonging to the free surface contour, as shown in Eq. 14.

$$\hat{n} = \hat{n}_w \cos\theta_w + \hat{t}_w \sin\theta_w \quad (14)$$

It is known [13] that when the Brackbill model is implemented in the two-fluid Eulerian-Eulerian approach, the force must be divided between the two fluid phases occupying each cell. The reason for this is that both momentum equations are solved in the system. The pressure gradient in the two fluid model is calculated by the sum of the momentum equations. This gradient should be the same as the one in the single-fluid (homogeneous) model (Eq. 15). This means that the sum of both averaged factors ( $\beta_1, \beta_2$ ) must be one.

$$(\alpha_1 + \alpha_2) = (\beta_1 + \beta_2) \mathbf{M}^{ST} \quad (15)$$

Bartosiewicz [13] proposed two models for  $\beta_k$ , the first one based on mass average, and the second based on volume average in the cell. Strubelj [14] studied both models by analyzing the pressure jump over a droplet and concluded that the best results were given by the volume averaging model. The model in GENTOP has been implemented in the CFX code as a general momentum source in a similar manner as with the clustering algorithm, where the separation between the two fluids is given by this volume averaging model.

### 3. RESULTS AND DISCUSSION

#### 3.1. Analytical Study of Cubic and Ellipsoidal Ethanol Droplets

Based on the work of Strubelj [14] and Canot and Caltagirone [15], the first quantitative calculation cases are centered on analytical studies of oscillating droplets. Instead of the two-dimensional calculations presented in these previously-mentioned papers, three dimensional ethanol square ( $l = 40$  mm), and

ellipsoidal droplets ( $r_{\text{averaged}} = 22.56$  mm) are initially centered in a square cavity of  $L = 75$  mm surrounded by air, where a zero-gravity field is imposed. The flow is isothermal, and there is no changes on the surface tension coefficient. The fluid properties are  $\rho_1 = 787.88$  kg/m<sup>3</sup>,  $\mu_1 = 2.4 \times 10^{-2}$  Pa s for the ethanol, and  $\rho_2 = 1.1768$  kg/m<sup>3</sup>,  $\mu_2 = 2 \times 10^{-3}$  Pa s for the air. The objective behind increasing the viscosity values by a factor of 20 compared to the real viscosities, is to achieve higher dumping of spurious velocities and bubble shape oscillations, as well as faster stabilization. The surface tension between the ethanol and air is  $\sigma = 0.02361$  N/m. The oscillation period in the calculations of three-dimensional droplets with initially ellipsoid ( $n = 2$ ), and square shape ( $n = 4$ ) is compared to the approximated analytical solution given by Eq. 16 and Eq. 17. Here  $\omega_0$  is the oscillating frequency and  $\tau_0$  is the oscillating time period. The highest point in the axial direction or “north pole” is tracked in order to determine the oscillating period.

$$\omega_0^2 = \frac{(n^3 - n)\sigma}{(\rho_1 + \rho_2)R^3} \quad (16)$$

$$\tau_0 = \frac{2\pi}{\omega_0} \quad (17)$$

For the case in which an initial cubic shape is chosen with a relatively coarse mesh (32 x 32 cells within the droplet), the difference between the analytical and simulating solutions is only of 1.68 %, where the oscillating period on the calculation is 0.526 s, and in the analytical solution 0.535 s (Fig. 1). As expected, damping is larger in a coarse grid due to the discretization error in the convective part which acts as a diffusive term (numerical viscosity) in the momentum equation. As it was observed by Strublji in their two-dimensional cases, also here we observed a slightly changing with grid refinement which remains in the range of  $\pm 5$  %. As it can be seen from refining the mesh (128 x 128) in the cubic case, after 10 s of calculation the ethanol droplet is still oscillating. In this case, the oscillating period calculated from the simulation is around 0.536 s, which differs only in 0.19 % from the analytical solution (Fig. 2). This shown an improvement on the results of around 1.49 % by refining the mesh by a factor of 4.

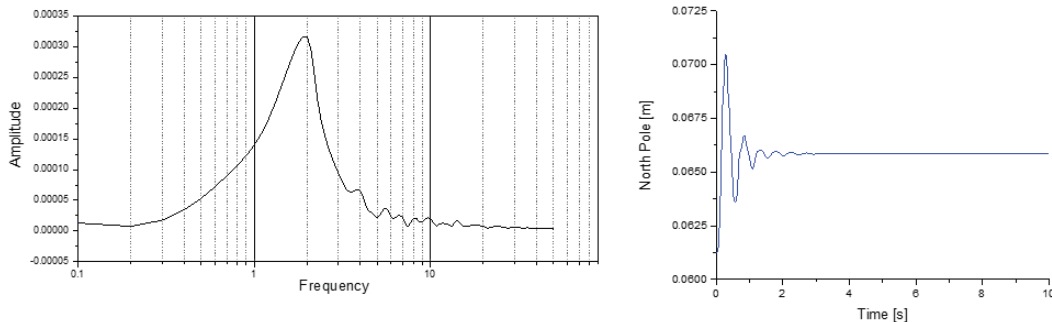


**Figure 1. Oscillating frequency for a initially cubic ethanol droplet in air (32 x 32)**

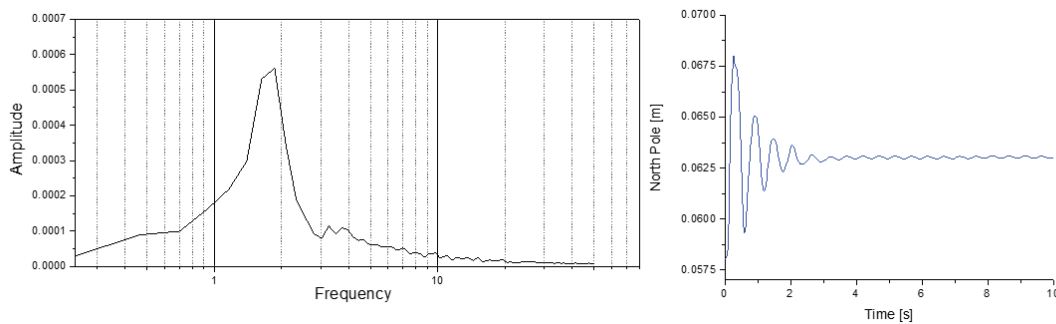


**Figure 2. Oscillating frequency for an initially cubic ethanol droplet in air (128 x 128)**

The ellipsoidal test case is naturally more challenging. When using the coarser mesh, the oscillating period obtained from the calculation is 1.12 s while the analytical solution is around 1.55 s which give a difference between the two results of 23 % (Fig. 3). Further, it appears as if the droplet slightly shifted position in the axial direction, which could be occurring due to parasitic air velocities affecting the droplet interface [14]. When the mesh is refined to 128 x 128, the droplet is no longer displaced. As with the refinement in the cubic case, the damping decreases obtaining a non-trivial oscillation even after 10 s of calculation. In this case, the oscillating period calculated from the simulation is around 1.25 s, which differs in 19.3% from the analytical solution (Fig. 4). This shown an improvement on the results of around 4.8% by the refinement of the mesh, which again goes accordingly to the previously discussed observations from Strublj [14].

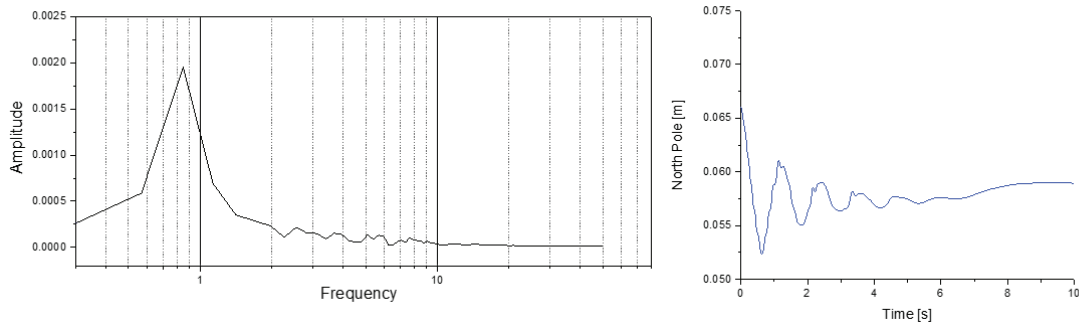


**Figure 3. Oscillating frequency for an initially elliptical ethanol droplet in air (32 x 32)**

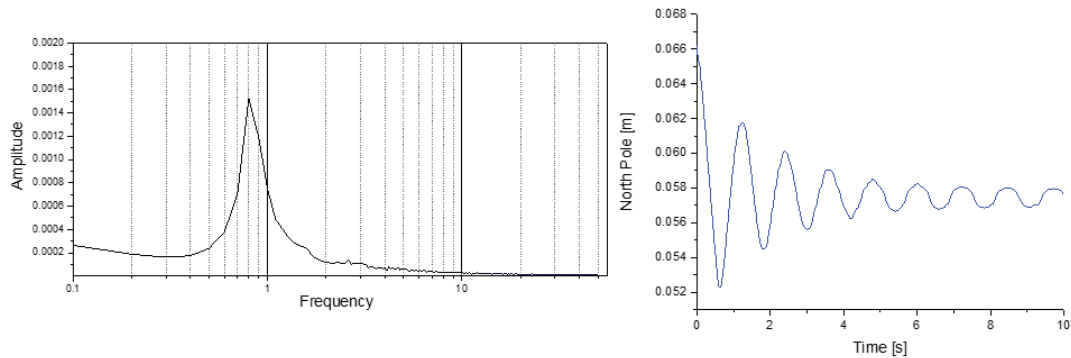


**Figure 4. Oscillating frequency for an initially elliptical ethanol droplet in air (128 x 128)**

### 3.2. Wall Adhesion Validation

Three different cases were simulated in order to test the contact angle section of the surface tension implementation for the GENTOP concept. The cases were based on a spherical drop of water residing on a wall-boundary surface (Fig.5). Gravity needs to be considered in these cases, and depending of the pre-defined contact angle (calculated from the inside of the droplet), the surface tension should be able to maintain the droplet standing with the proper inclination within the interface between the free surface and the wall. The complete domain, including the surroundings, in these cases counts with around 12 mm in length and a total of around three hundred thousand hexahedral cells. The diameter of the droplet is 4 mm.

The first contact angle which was defined was 30 degrees, and while it is not possible to observe the result in a static image; the droplet starts opening while the vectors of the surface tension force pushed towards the outside of the free surface, until the residing angle of 30 degrees has been achieved. At this point the force changes direction and acts to maintain the pre-defined contact angle (Fig. 6).

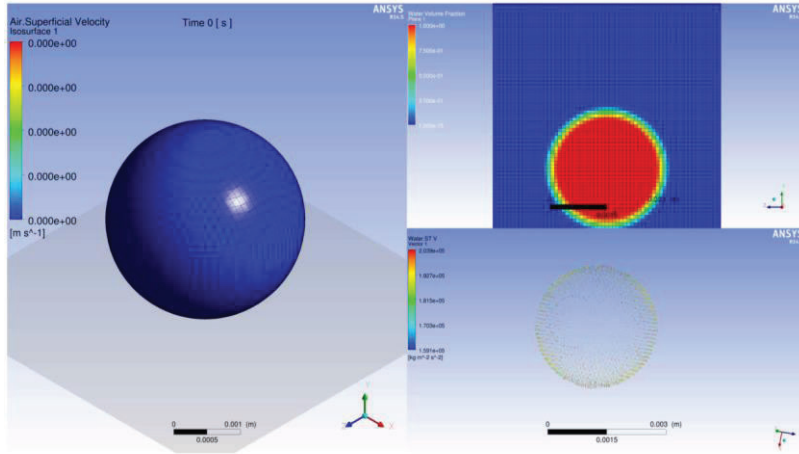


**Figure 5. Initial state for calculations of contact angle for a residing bubble**

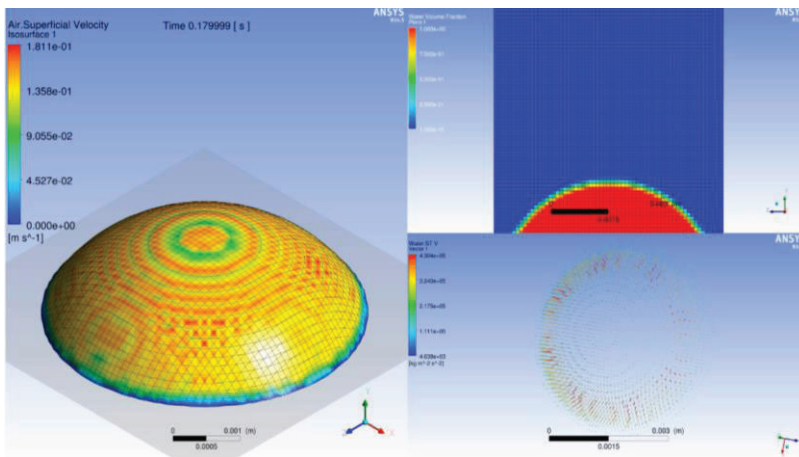


**Figure 6. Final state for calculations for a residing bubble with a contact angle of 30°**

In the second case, a residing angle of 90 degrees was established. In a similar manner as in the previous test, the contact angle was successfully achieved within the first 0.1 s and maintained during the rest of the 0.6 s of calculation (Fig. 7). Finally, an extreme case with a contact angle of 179 degrees was tested to check the implementation limits, obtaining a final residing angle of around 168 degrees (Fig. 8).

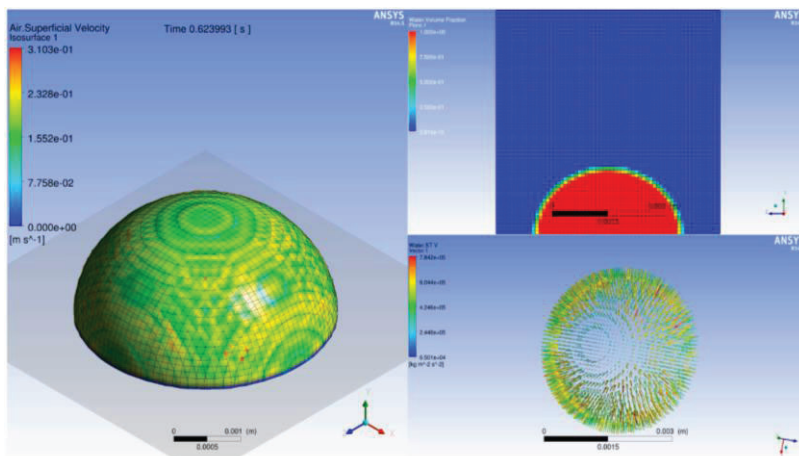


**Figure 7. Final state for calculations for a residing bubble with a contact angle of 90°**

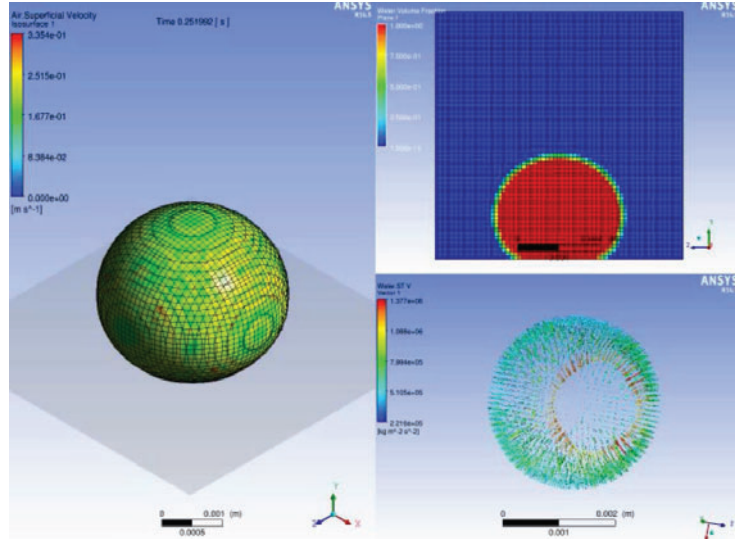


Figure 8. Final state for calculations for a residing bubble with a contact angle of 179°

### 3.3. Rising Bubble Morphology and Velocity Validation

Tomiya [16] has rigorously quantified the shapes and velocities of single bubbles rising through a vertical pipe. The experiments were performed with air-water and a 24.8 mm pipe length. The ratio,  $\lambda$ , of equivalent bubble diameter ( $d_B$ ) to the diameter of the tube ( $D_T$ ) was varied from 0.2 to 2.0 in these experiments. In this work, the test case for  $\lambda = 0.6$  for stagnant and pipe flow have been simulated and are discussed. When bubbles have a ratio  $\lambda$  greater than 0.6, they are usually classified as Taylor bubbles and their terminal velocity is no longer a function of  $\lambda$ , but of  $D_T$ . In these cases, the terminal velocity can be expressed as in Eq. 18, where  $Fr$  represents the Froude number which is a function of the Eötvös and Morton numbers.

$$V_T = Fr^3 \sqrt{\frac{(\rho_l - \rho_g)gD}{\rho_l}} \quad (18)$$

The correlation suggested by Nicklin [17] and Collins [18] for a Taylor bubble is used, and can be expressed as in Eq. 19.

$$V_B = C\bar{V}_L + V_T \quad (19)$$

Where the constant  $C$  can be calculated for  $Re > 2,300$  as shown in Eq. 20.

$$C = 1.18 + 0.32 \exp[0.0017(2300 - Re)] \quad (20)$$

For the current cases, the terminal velocity value for the stagnant fluid,  $V_T$ , should have a theoretical value of 0.216 m/s. The bubble velocity for the pipe flow case,  $V_B$ , was calculated as 1.396 m/s when the liquid velocity was defined as 1 m/s.

Finally, Tomiyama also proposed an analytical model to study the shape of the bubbles, as shown in Eqs. 21 - 24, where  $R_{int}$  is the radius of the bubble interface, and  $Z$  is the distance from the nose of a bubble directed downward.

$$R_1^* = 9 - [Z^{*0.7} + 0.9^{1/a}]^a \quad (21)$$

$$R_2^* = \frac{R_{int}}{R} \quad (22)$$

$$Z^* = \frac{Z}{R} \quad (23)$$

$$a = \min(3.26 \times 10^{-4} Re_L - 2.83, 2.29 \times 10^{-5} Re_L - 2.36) \quad (24)$$

The first test was performed on a representative mesh, using 24 cells in the radial direction, and a time step of  $1e-4$  s. Since stagnant flow was chosen, it assumes laminar flow conditions. A constant drag coefficient of 0.44 was set for this calculation. In order to separate the effects of all other forces in GENTOP and study only the effect of the surface tension implementation, the inhomogeneous “free surface” model inherit from CFX with aggressive interface compression scheme was used.

For this first case, the surface tension has been deactivated. As the bubble rises in the channel, the shape and interface is highly disturbed, and the gas structure is in constant oscillation. This is consistent with the behavior observed in the GENTOP validation on the MT-Loop pipe flow cases [1]. The terminal velocity was found to be 0.219 m/s, deviating from the theoretical solution by only 1.38 %. In terms of the morphology of the bubble, Fig. 9, shown a very deformed structure which is certainly not expected for this case. A comparison using the Tomiyama analytical model in this case, would yield unphysical results.

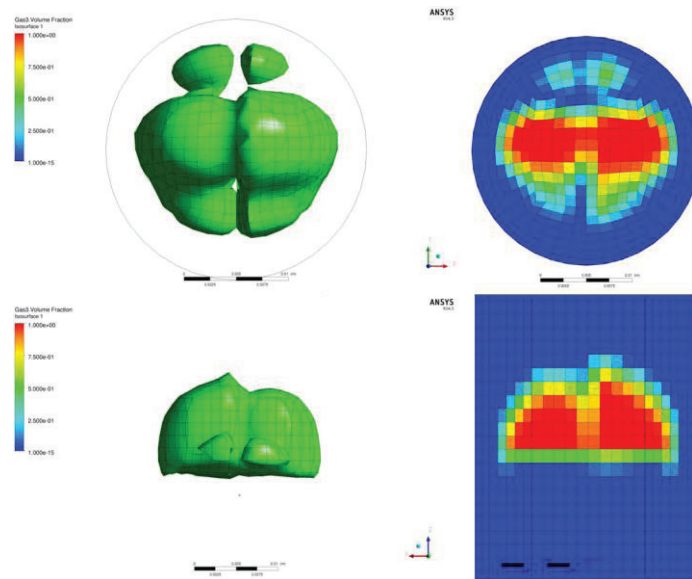


**Figure 9. Morphology of a single rising bubble of  $\lambda = 0.6$  without surface tension**

When the newly implemented surface tension is activated, the shape of the bubble greatly improves, obtaining the expected cap-like gas structure. When the analytical Tomiyama model is used the error between the analytical and calculating results is only 0.41 % for this case (Fig. 10). Here, the velocity hardly changes compared to the previous test, obtaining a value of 0.221 m/s.

When liquid velocity is included ( $V_L = 1$  m/s), the Re number grows to about 28,000. Here, the resolution of the bubble within the free surface seems to be reduced, and the difference between the analytical and calculated results for the morphology differs in about 13.7% at the end of the channel (Fig. 11). The inclusion of the liquid velocity shown an approximation to the analytical bubble velocity, as given by Eq. 19, of  $V_B$  equal to 1.30 m/s and a difference with the theoretical result of 6.8%.

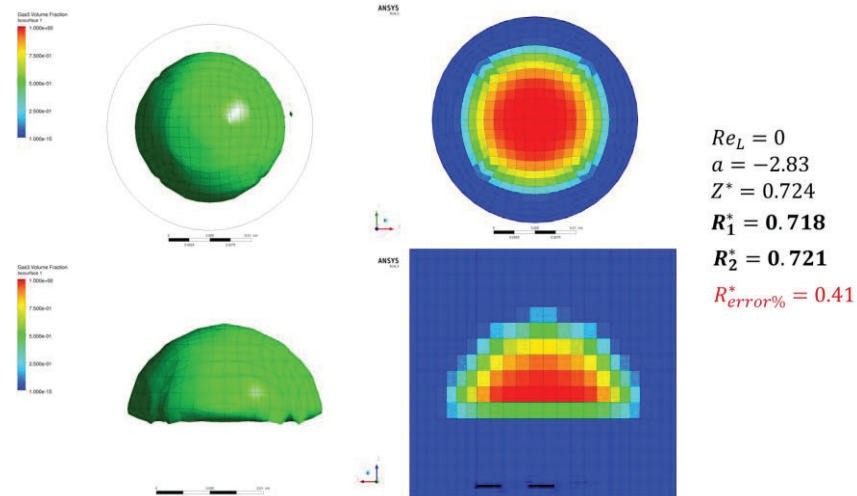


**Figure 10. Morphology study of a single rising bubble of  $\lambda = 0.6$  with the surface tension implementation**

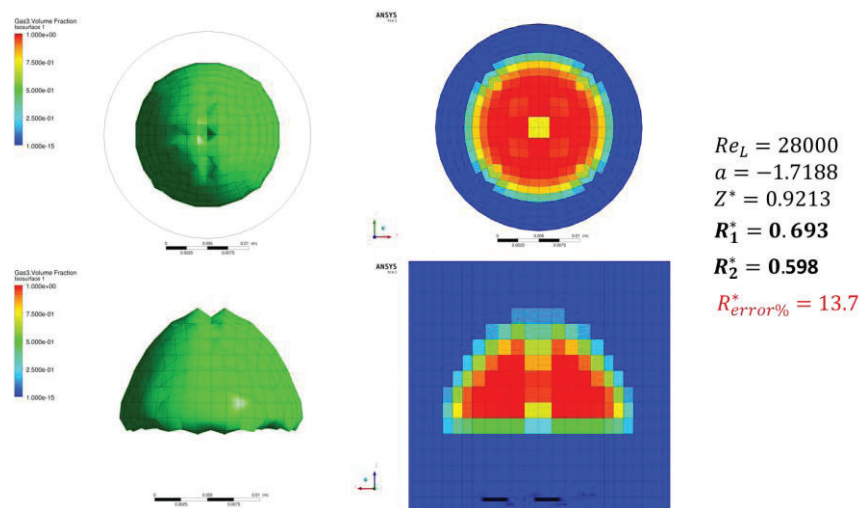


**Figure 11. Morphology study of a single rising bubble of  $\lambda = 0.6$  with the surface tension implementation and  $V_L = 1.0$  m/s**

Finally, the test case for  $\lambda = 0.6$  and stagnant liquid conditions, was replicated using the full GENTOP concept. For this, two gas-fields were defined, where Gas3 represents the potentially-continuous field, and Gas2 represents the polydispersed structures. Seven iMUSIG size groups were used, and  $D_{dg,max}$  was defined as 5.8 mm based on the sign change of the Tomiyama lift coefficient. As it can be observed from Fig. 12, the full GENTOP concept, including the surface tension, allows a much improved resolution of the continuous gas, and even without an interface compression scheme the surface tension force is strong enough to maintain the interface sharp. It can also be seen that, while there is some small shearing of the continuous gas, only a limited part is converted into dispersed ( $\alpha_{Gas2} < 0.0022$ ), which is what it would be expected in this test case for which only Gas3 has been initialized. In terms of bubble morphology, there is only a small deviation from the analytical solution, 1.1 %. In terms of velocities, contrary to the other two cases where a constant drag of 0.44 was defined, the AIAD drag coefficient for the free surface seems to highly underpredict the rising velocity on the calculation resulting in 0.135 m/s, showing that, a more classic coefficient of 0.44 for the free surface region on GENTOP instead of the full AIAD model could be sufficient for the proper prediction of velocity distribution for the resolved gas in vertical flow conditions.

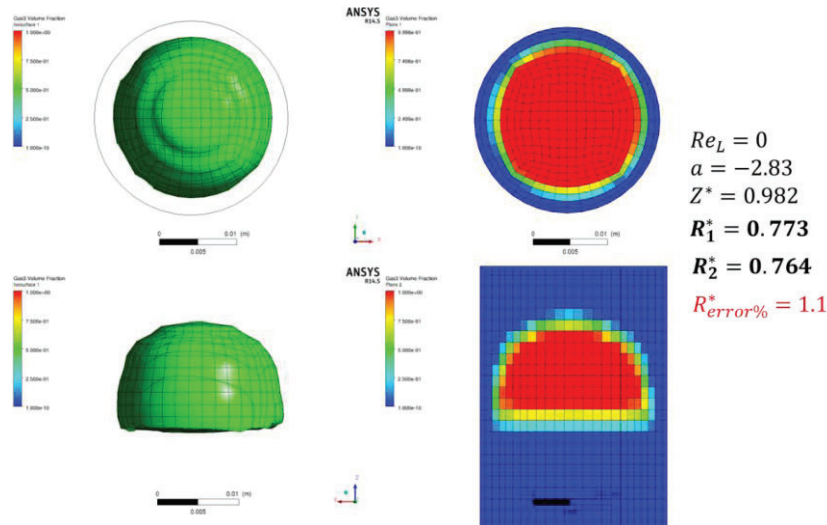


**Figure 12. Morphology study of a single rising bubble of  $\lambda = 0.6$  with the surface tension implementation using the full GENTOP concept**

#### 4. CONCLUSIONS

The work presented in this paper has shown the importance of including a proper surface tension force model in the GENTOP concept. The implementation of surface tension in GENTOP was first tested for an ethanol droplet suspended in air, with void initialization from a cubic and ellipsoidal shape. The maximum deviations from the analytical models were 1.68 % for the cubic case and 23 % for the ellipsoidal case. Refinement of the mesh by a factor of four, yields an improvement of the results lower than 5% in both cases. A wall adhesion model was also included with the surface tension implementation and successfully validated against three different contact angles of 30°, 90°, and 179° for a residing droplet. Finally, the model was tested against analytical and experimental solutions for a rising single gas bubble morphology and flow velocity  $V_L = 0$  m/s and  $V_L = 1.0$  m/s. In terms of bubble shape predictions the cases under stagnant flow conditions show a maximum error of 1.1 % for the morphology comparison against the analytical results, while the pipe flow case presented a deviation of 13.7 %. In term of rising velocity, the cases based on stagnant flow, with a constant drag of 0.44 produce a deviation from the theoretical solution of only 0.4%. The GENTOP couple to the AIAD drag concept shows a larger under prediction of the rising velocity. The performed analysis have clearly evidenced improved bubble resolution for the surface tension enable GENTOP model in comparison to the “Free Surface” inhomogeneous model with aggressive interface compression scheme. Finally, the surface tension has allowed to partially diminish the artificial effect caused by the clustering method by adding a more physical meaning to the formulation as soon as the critical gradient of volume fraction in  $\varphi_{fs}$  has been reached.

#### ACKNOWLEDGMENTS

This work was carried out in the framework of a research project funded by E.ON Kernkraft GmbH. The authors would also like to acknowledge the support received from the DOE Sponsored Consortium for Advance Simulation of Light Water Reactors (CASL).

#### REFERENCES

1. Montoya, G.; Lucas D.; Krepper, E.; Hänsch, S.; Baglietto, E. “Analysis and Applications of a Generalized Multi-Field Two-Fluid Approach for Treatment of Multi-Scale Interfacial Structures in

- High Void Fraction Regimes”. Proc. Int. Congress on Adv. on Nucl. Power Plants. ICAPP2014-14230, USA (2014).
2. Rzehak, R.; Krepper, E. “Closure models for turbulent bubbly flows: A CFD study”. Nucl. Eng. Des., 265: 701-711 (2013).
  3. Hänsch, S.; Lucas, D.; Krepper, E.; Höhne, T. “A multi-field two-fluid concept for transitions between different scales of interfacial structures”. Int. J. Mult. Flow 47:171-182 (2012).
  4. Ishii, M.; Zuber, N. “Drag Coefficient and Relative Velocity in Bubbly, Droplet or Particle Flows”. AIChE J., 25: 843-855 (1979).
  5. Tomiyama, A.; Tamai, H.; Zun, I.; Hosokawa, S. “Transverse Migration of Single Bubbles in Simpler Shear Flows”. Chem. Eng. Sci., 57: 1849-1858 (2002).
  6. Tomiyama, A. “Struggle with Computational Bubble Dynamics”. Proceedings International Conference on Multiphase Flow, France (1998).
  7. Hosokawa, S.; Tomiyama, A.; Misaki, S.; Hamada, T. “Lateral Migration of Single Bubbles Due to the Presence of Wall”. ASME 2002 Joint U.S.-European Fluids Engineering Division Conference. Montreal, QC, Canada (2002).
  8. Burns, A.D.B.; Frank, Th.; Hamill, I.; Shi, J.M. “The Favre Averaged Drag Model for Turbulent Dispersion in Eulerian Multi-Phase Flows”. 5<sup>th</sup> International Conference on Multiphase Flow. Yokohama, Japan (2004).
  9. Höhne, T.; Deendarlianto; Lucas, D. “Numerical simulations of counter-current two-phase flow experiments in a PWR hot leg model using an area density model”. Int. J. Heat Fluid Flow 31 (5): 1047-1056 (2011).
  10. Prince, M.J.; and Blanch, H.W. “Bubble Coalescence and Break-Up in Air-Sparged Bubble Columns”. AIChE J., 36(10): 1485-1499 (1990).
  11. Luo, H; Svendsen, H.F. “Theoretical model for drop and bubble break-up in turbulent flows”. AIChE J., 42(5): 1225-1233 (1996).
  12. Brackbill, J. U.; Kothe, D.B.; Zemach, C. A. “A continuum method for modeling surface tension”. J. Comput. Phys. 100: 335-354 (1992).
  13. Bartosiewicz, Y.; Lavieville, J.; Seynhaeve, J.M. “A first assessment of the NEPTUNE\_CFD code: instabilities in a stratified flow comparison between the VOF method and a two-field approach”. Int. J. of Heat and F. Flow 29 (2): 460-478 (2008).
  14. Strublj, L.; Tiselj, I.I Mavko, B. “Simulations of free surface flows with implementation of surface tension and interface sharpening in the two-fluid model”. Int. J. of Heat and Fluid Flow. 30: 7741-750 (2009).
  15. Canot, E., Caltagirone, J.-P. “Test-case no. 10: parasitic currents induced by surface tension (PC)”. Multiphase Science and Technology 16, 69–74 (2004).
  16. A. Tomiyama, et al. “Rising Velocities and Shapes of Single Bubbles in Vertical Pipes” Proc. ICMF, New Orleans, USA (2001).
  17. Nicklin, D.J.; Wilkes, J.O.; Davidson, J.F. “Two-phase flow in vertical tubes”. Inst. Chem. Eng. 40-1: 61-68 (1962).
  18. Collins, R.; De Moraes, F.F; Davidson, J.F.; Harrison, D. “The motion of a large gas bubble rising through liquid flowing in a tube”. J. Fluid Mech. 89-3: 497-514 (1978).